How does the rotational direction of an upwind turbine affect its downwind neighbour?

How does the rotational direction of an upwind turbine affect its downwind neighbour?

Antonia Englberger[1], Linus Wrba[1], Andreas Dörnbrack[1], Julie K. Lundquist[2,3]

[1]Institut für Physik der Atmosphäre, DLR Oberpfaffenhofen, Germany.
[2]Department of Atmospheric and Oceanic Sciences, University of Colorado Boulder, Boulder, USA.
[3]National Renewable Energy Laboratory, Golden, Colorado, USA.

Author contact email: antonia.englberger@dlr.de

Keywords: wakes

Abstract

Wind-turbine blades rotate in clockwise direction looking downstream on the rotor. During daytime conditions of the atmospheric boundary layer, the rotational direction has no influence on the turbine wakes. In stably stratified conditions occurring during night, the atmospheric inflow is often characterized by a veering inflow describing a clockwise wind direction change with height in the Northern Hemisphere. A changing wind direction with height interacting with the rotor impacts its wake characteristics (wake elongation, width and deflection). We investigate the impact on the turbine performance (streamwise velocity for power, turbulence kinetic energy for loading) of a downwind turbine considering the four possible combinations of rotational directions of two 5 MW NREL rotors by means of large-eddy simulations. A counterclockwise rotating upwind turbine results in a 4.1% increase of the rotor averaged inflow velocity at the downwind rotor in comparison to a common clockwise rotating upwind turbine rotor. In case of two counterclockwise rotating rotors, the increase is 4.5%. This increase in streamwise velocity is accompanied by a 3.7% increase in rotor averaged turbulence kinetic energy. The performance difference of the downwind rotor (+4.8% increase of cumulative power of both wind turbines, if the upwind rotor rotates counterclockwise) results from the rotational direction dependent amplification or weakening of the spanwise and the vertical wind components, which is the result of the superposition of veering inflow and upwind rotor rotation.

1 Introduction

Wind turbines operating in a stably stratified atmospheric boundary layer interact with a vertically sheared wind, which is often superposed by a veering wind. A veering wind is characterized by a clockwise (counterclockwise) wind direction change with height in the Northern (Southern) Hemisphere. The veering of the wind in the stable boundary layer (SBL) is described by the Ekman spiral and can be attributed to the interaction between the Coriolis force and friction. Previous studies show an impact of the rotational direction of a wind turbine on its wake under veering inflow [5, 3, 4], whereas it is of minor importance for an unidirectional wind over the whole rotor [6, 5]. The wake under veering inflow has a larger streamwise elongation, a narrower spanwise width, and a smaller

deflection angle in case of a common clockwise rotating rotor in the Northern Hemisphere. This impact of the rotational direction under veering inflow results from an amplification of the spanwise velocity component of the near wake in case of a counterclockwise rotating rotor. In case of a clockwise rotating rotor, the spanwise velocity component is weakened and can even reverse sign [5].

These previous studies [5, 4] are limited to the wake of a single wind-turbine rotor. This approach is extended in this study, which focus on the wakes of a pair of rotors, aiming to answer the following question: How does the rotational direction of an upwind turbine affect its downwind neighbour? To answer this question, we investigate the rotational direction impact of the upwind turbine on the performance of the downwind turbine. Therefore, we focus on the streamwise velocity as a measure of the power production of the downwind turbine and on the turbulence kinetic energy in the flow, which can be related to turbine loading. Both parameters are analyzed for the 5 MW NREL rotor. Further, we analyze the rotational direction impact of a pair of co- and counter-rotating turbines on its wakes. All investigations are performed under sheared and veered atmospheric inflow by means of large-eddy simulations (LESs).

The paper is organized as follows: After describing the framework in Sect. 2, the wake structure is investigated in Sect. 3.1, the performance of the downwind turbine in Sect. 3.2, and a root case analysis follows in Sect. 3.3. The conclusion is presented in Sect. 4.

2 Framework

The dry stably stratified atmospheric boundary-layer flow through an array of two wind turbines is simulated with the multiscale geophysical flow solver EULAG [8]. The numerical simulations solve the Boussinesq equation for the Cartesian velocity components u, v, w and for the potential temperature perturbation $\Theta^{'} = \Theta - \Theta_e$ [12],

$$\frac{d\mathbf{v}}{dt} = -\boldsymbol{\nabla}\left(\frac{p^{'}}{\rho_0}\right) + \mathbf{g}\frac{\Theta^{'}}{\Theta_0} - 2\,\Omega_C\,(\mathbf{v} - \mathbf{v}_e) + \boldsymbol{\beta}_{\mathbf{v}}\frac{\mathbf{F}_{WT}}{\rho_0} + \boldsymbol{\mathcal{V}}, \tag{1}$$

$$\frac{d\Theta^{'}}{dt} = -\mathbf{v}\nabla\Theta_e + \mathcal{H}, \tag{2}$$

$$\boldsymbol{\nabla}\cdot(\rho_0\mathbf{v}) = 0, \tag{3}$$

with Θ_e representing the environmental state and Θ_0 a constant reference value of 300 K. Further, d/dt represent the total derivative, $\boldsymbol{\nabla}$ the gradient, $\boldsymbol{\nabla}\cdot$ the divergence, $p^{'}$ the pressure perturbation with respect to the environmental state, $\rho_0 = 1.1$ kg m^{-3} is used as constant density, and $\mathbf{g}$ represents the vector of acceleration due to gravity. The Coriolis force is considered via the angular velocity vector Ω_C of the rotation of the earth. The simulations are performed with a turbulence kinetic energy closure following [14] with the corresponding subgrid-scale terms $\boldsymbol{\mathcal{V}}$ and $\mathcal{H}$ of viscous dissipation of momentum and diffusion of heat.

The wind-turbine induced forces $\mathbf{F}_{WT}$ are parameterized with the blade element momentum method as rotating actuator disc following [7], which can rotate clockwise ($\beta_v = 1$, $\beta_w =$ -1) and counter-clockwise ($\beta_v =$ -1, $\beta_w = 1$). In this study we performed the simulations for the 5 MW NREL rotor with a rotor diameter of $D = 126$ m and a hub height of $z_h = 90$ m, a turbine spacing of 7 D, and a spatial resolution of 5 m (resolution of atmospheric input data from precursor simulation). Four simulations are conducted, two clockwise rotating turbines (CR CR), two counterclockwise rotating turbines (CCR CCR), and two simulations with one co- and one counter-rotating turbine (CR CCR and CCR CR).

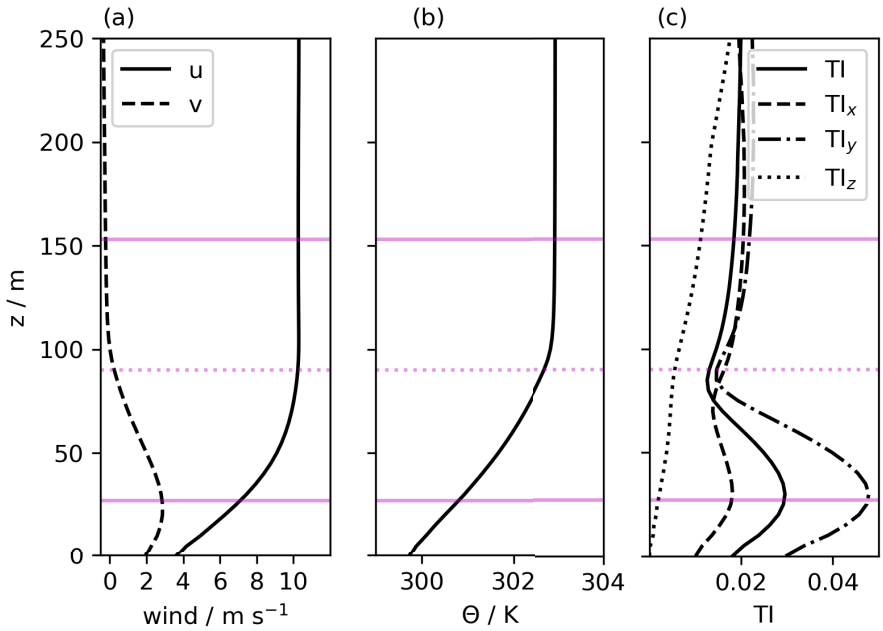

Figure 1: Vertical profiles of the zonal u and meridional v wind component in (a), the potential temperature Θ in (b), and the total turbulent intensity TI (Eq. 6) with its three components in streamwise (TI_x), spanwise (TI_y), and vertical (TI_z) direction.

The simulations are initialized with a stably stratified flow regime, which is extracted from a diurnal cycle simulation [2]. The turbulent inflow is integrated into the wind-turbine simulations with open streamwise boundary conditions by a synchronized coupling. For a more detailed description of this method we refer to [5]. The horizontal averaged atmospheric inflow profiles of the zonal and meridional wind components u and v, the potential temperature Θ, and the turbulent intensity TI including the three individual components (TI_x, TI_y, TI_z) are shown in Fig. 1. The colored dotted lines represent the hub height of the wind turbine and the solid lines incorporate the atmospheric region from bottom to top tip, interacting with the rotating rotor.
For the investigation of the wake characteristics, 10 min time averaged values of the streamwise velocity $\overline{u_{i,j,k}}$ and the spanwise velocity $\overline{v_{i,j,k}}$ at the corresponding grid point i, j, k are used. Further, we refer to:

- the velocity deficit:

$$VD_{i,j,k} \equiv \frac{\overline{u_{1,j,k}} - \overline{u_{i,j,k}}}{\overline{u_{1,j,k}}}, \tag{4}$$

- the turbulence kinetic energy:

$$TKE_{i,j,k} = 0.5(\overline{u'^2_{i,j,k}} + \overline{v'^2_{i,j,k}} + \overline{w'^2_{i,j,k}}), \tag{5}$$

  with $u'_{i,j,k} = u_{i,j,k} - \overline{u_{i,j,k}}$ respectively

- the turbulence intensity

$$TI_{i,j,k} = \frac{TKE_{i,j,k}}{\overline{u_{i,j,k_h}}} \tag{6}$$

  with k_h representing the grid point of the turbine rotor hub height z_h.

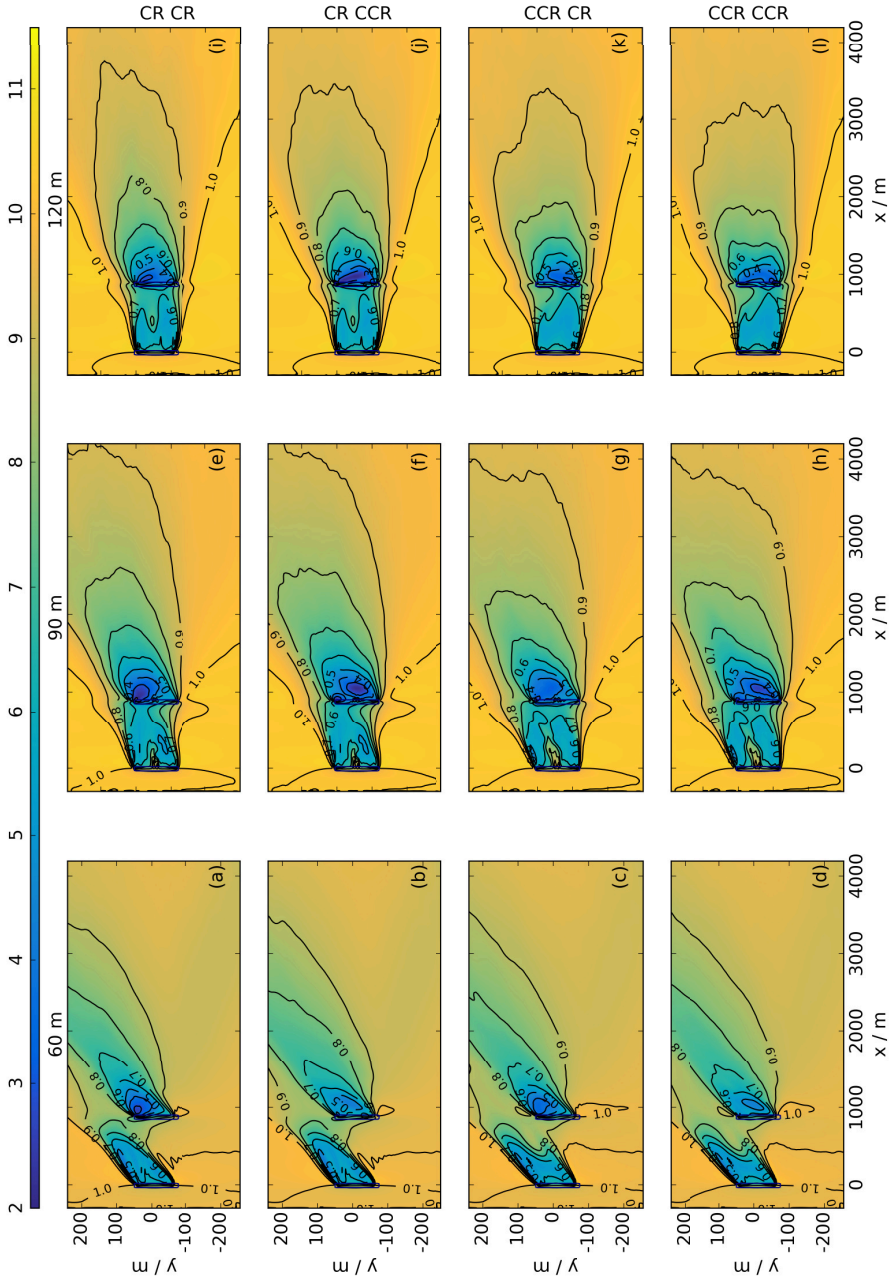

Figure 2: Coloured contours of the 10 min temporal averaged streamwise velocity in meters per second at 60 m (left column), 90 m (center) and 120 m (right column) for four combinations of rotational direction arrangements (CR CR in first row, CR CCR in second row, CCR CR in third row, CCR CCR in last row). The black contours represent the velocity deficit (Eq. 4).

3 Results

3.1 Wake Structure

The impact of the upwind turbine on its downwind neighbour is investigated in detail. Figure 2 represents the time averaged streamwise velocity $\overline{u}$ at three different heights (lower (60 m) and upper (120 m) rotor part and hub height (90 m)) with the four possible combinations of clockwise (CR) and counterclockwise (CCR) rotor rotation for two wind turbines. At first view, the wakes of the two turbines are similar, independent of the rotational direction. But there are significant differences looking at Fig. 2 in detail. The wake of the upwind rotor shows a larger width (Fig. 2(g, h, k, l)) and a larger deflection angle (Fig. 2(c, d, k, l)) in case of a counterclockwise rotating rotor. This agrees with previous studies [5, 4], which discuss the same nighttime veering inflow condition interacting with a single scaled wind turbine. The wake deflection angle difference results in larger (smaller) streamwise velocity values at the downwind rotor position for $y < 0$ ($y > 0$) in case of a CCR upwind rotor, especially pronounced at hub height and in the upper rotor half (Fig. 2(g, h, k, l)).

Considering the resulting wake of the downwind rotor, there are also differences in the velocity deficit (Eq. 4), the streamwise elongation, the spanwise width, and the deflection angle of the wake. This time, however, they are influenced by the combination of both rotational directions of the turbines. Starting with the velocity deficit behind the second turbine at 60 m height (Fig. 2 first column). If the second turbine rotates clockwise, the velocity deficit reaches smaller values in comparison to a counterclockwise rotating downwind rotor (CR CR and CCR CR compared to CR CCR and CCR CCR). Further, in case of the combination CCR CR, the minimum value of the velocity deficit is 0.4, whereas in case of CR CR it is reduced to 0.3. This suggests, that the deceleration effect is intensified, if both rotors rotate clockwise. The same is valid in the upper rotor part (last column). The wake elongation, the wake width, and the wake deflection angle difference follow the same pattern. If both rotors rotate counterclockwise, the deflection angle and the spanwise width of the second wake reaches largest values, whereas its streamwise elongation reaches smallest values. To give an example, at 90 m height the difference between CR CR and CCR CCR at the downwind wake shows an $\approx 1/3$ larger wake deflection angle, an $\approx 1/6$ larger spanwise wake width, and an $\approx 1/3$ smaller streamwise wake elongation for CCR CCR.

3.2 Performance of the downwind turbine

For a more quantitative comparison of the four combinations and especially the impact of the rotational direction on the performance of the second rotor, the difference $u-u_{ref}/u_{ref}$ is calculated as a downstream function in Fig. 3 (left column), whereas the common combination of two clockwise rotating rotors is considered as reference case u_{ref}. Considering the upper rotor half in (a), the streamwise velocity interacting with the second wind turbine increases up to 9.5% in case of a counterclockwise rotating upwind rotor in comparison to a clockwise one. The effect is slightly less pronounced, if both rotors rotate counterclockwise. Considering the lower rotor half in (c), the rotational direction impact of the upwind rotor is much smaller at the location of the second rotor. This can be explained with the inflow wind direction in the lower rotor half (Fig. 1(a)), resulting in a mainly non-waked inflow and therefore in a less pronounced impact of the upwind rotor (Fig. 2 (first column)). The percentage differences at the position of the downwind turbine are listed for all three cases in Table 1. Concluding, the velocity ratio $u-u_{ref}/u_{ref}$ averaged over the whole rotor (Fig. 3(b)) results in a 4.5% (4.1%) higher inflow velocity interacting with a counterclockwise (clockwise) rotating second rotor in case of a counterclockwise rotating upwind rotor. Table 2 further lists the relative cumulative power production. It is calculated as the ratio of the cumulative power production of the

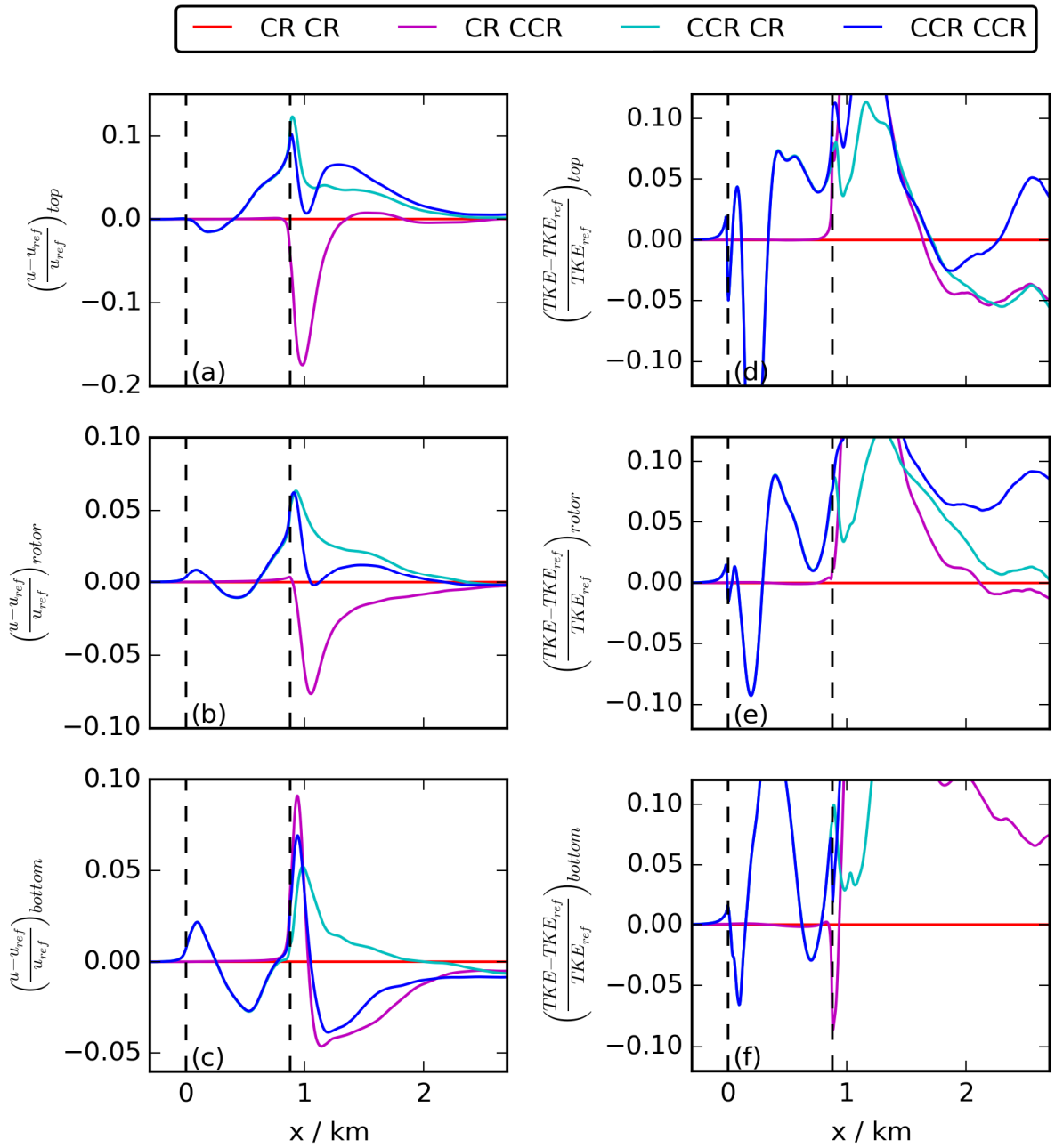

Figure 3: Downstream evolution of the velocity fraction $^{u-u_{ref}}/_{u_{ref}}$ (left column) and the turbulence fraction $^{TKE-TKE_{ref}}/_{TKE_{ref}}$ (right column). The first row represents the rotor top average, the last row the rotor bottom average, and the centered one the average over the whole rotor. The vertical dashed lines are the rotor positions.

new arrangement of the two turbines (e.g. CCR CCR) and two clockwise rotating wind turbines as reference cumulative power production. The rotational direction of the upwind turbine did not influence the rotor averaged velocity of the upwind turbine and therefore the produced power. However, it influences the rotor averaged velocity of the downwind turbine, resulting in a 4.8% increase of the cumulative power if the upwind rotor rotates counterclockwise instead of clockwise.

Table 1: Percentage differences resulting from the fraction $^{u-u_{ref}}/_{u_{ref}}$ at the downwind turbine, extracted from Fig. 3 (left column).

	$(\overline{^{u-u_{ref}}/_{u_{ref}}})_{top}$	$(\overline{^{u-u_{ref}}/_{u_{ref}}})_{bottom}$	$(\overline{^{u-u_{ref}}/_{u_{ref}}})_{rotor}$
CR CCR	-2.7%	+2.9%	+0.3%
CCR CR	+9.5%	+0.6%	+4.1%
CCR CCR	+8.8%	+2.2%	+4.5%

Table 2: Relative cumulative power production $^{P}/_{P_{ref}}$ for various combinations of rotational direction of two wind turbines and also of four wind turbines.

2 WT	$^{P}/_{P_{ref}}$	$^{P}/_{P_{ref}}$	4 WT
CR CCR	+0.3%	-1%	CR CCR CR CCR
CCR CR	+4.8%	+1.9%	CCR CCR CCR CCR
CCR CCR	+4.8%		

The difference $^{u-u_{ref}}/_{u_{ref}}$ is presented in Fig. 4(a) with N at the x-axis corresponding to $y>0$ in Fig. 2 calculated 15 m in front of the downwind turbine position with u_{ref} representing a common CR upwind rotor and u a CCR rotor. It is not shown directly at the position of the downwind turbine, as the actuator disc parametrization applies a smearing of the forces in x-direction mainly affecting two neighbouring grid points [1]. Figure 4 represents the case of two counterclockwise rotating rotors compared to two clockwise rotating ones. The case of a counterclockwise rotating upwind and a clockwise rotating downwind rotor (CCR CR) is not presented, as the fraction plot is rather similar to CCR CCR in Fig. 4. The arising regions of fraction values larger (smaller) than zero directly correspond to the discussed wake differences in front of the downwind rotor position for $y>0$ ($y<0$) in Fig. 2 and are the consequence of the wake deflection angle difference amplified by the wake width difference.

The rotational direction impact on $\overline{u}$ and therefore on the power is related to an impact on TKE and therefore on the loading acting on the downwind rotor. Therefore, the fraction $^{TKE-TKE_{ref}}/_{TKE_{ref}}$ is plotted as a downstream function in Fig. 3 (right column) with the common combination of two clockwise rotating wind turbines representing TKE_{ref}. The turbulence fraction shows more variability in streamwise direction in comparison to the streamwise velocity (first column). At the position of the downwind turbine, the rotor averaged turbulence fraction in Fig. 3(e) is higher in case of a counterclockwise rotating upwind rotor, an effect, which is accompanied by a larger velocity fraction in Fig. 3(b). The higher fraction value occurs in the upper (Fig. 3(d)), as well as in the lower rotor half (Fig. 3(f)).

A spatial distribution of the turbulence fraction is presented in Fig. 4(b), comparing CCR CCR to CR CR. In general, it can be stated that an increase of the streamwise velocity (Fig. 4(a)) accompanies an increase in TKE (Fig. 4(b)). Averaged over the rotor area, the difference between CCR CCR and CR CR is 3.7%, which will impact turbine loading of the downwind rotor.

3.3 Root Case Analysis

The observed differences of the streamwise velocity and consequently the TKE interacting with the second rotor result from the differences in the spanwise and vertical wake components. Figure 5

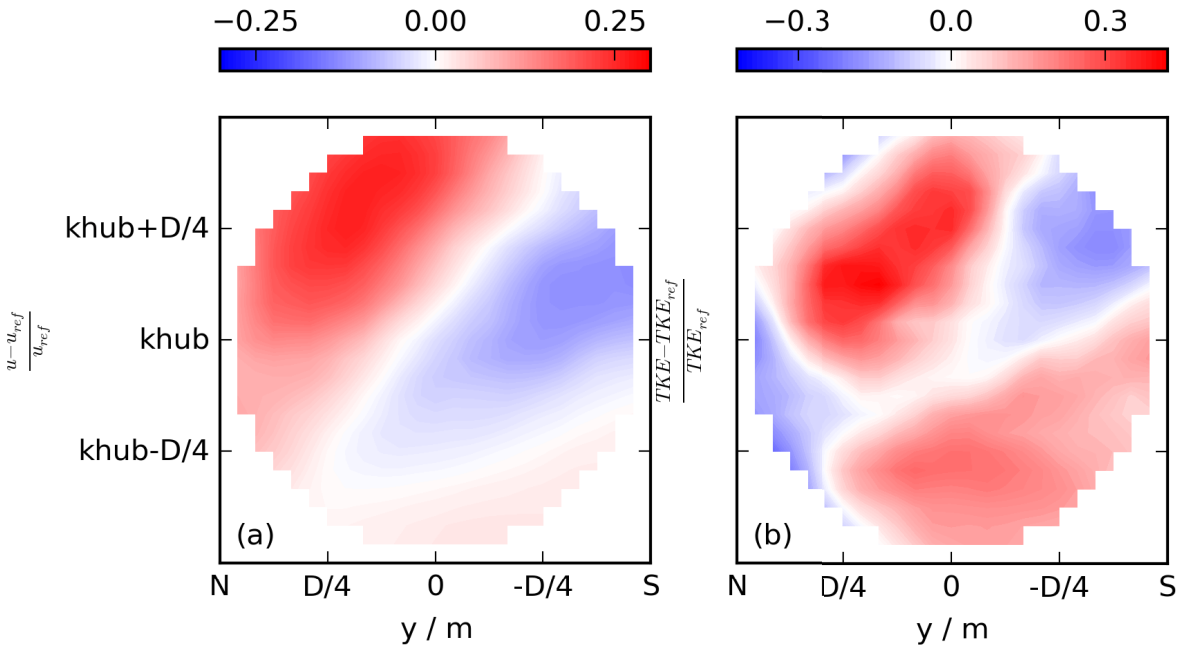

Figure 4: The fractions $u-u_{ref}/u_{ref}$ in (a) and $TKE-TKE_{ref}/TKE_{ref}$ in (b) at a position 15 m upstream of the second rotor. With N on the left, the viewer is looking from the first rotor downwind on the second rotor.

(left column) represents the averaged v-component of the upper rotor half (a), the lower rotor half (c), and over the whole rotor (b). In the upper rotor half (Fig. 5(a)), the amount of v at both rotor positions is the same, as the contribution of the inflow velocity v of the SBL is roughly zero (Fig. 1(a)). Positive (Negative) values of $\overline{v_{top}}$ result from a positive (negative) vortex component $v_{vortex} > 0$ ($v_{vortex} < 0$) in case of a clockwise (counterclockwise) rotating rotor. In the lower rotor half (Fig. 5(c)), v_{botom} is not symmetric for both rotational directions due to a changing inflow wind direction at the lower rotor half (Fig. 1(a)). In case of a common clockwise rotating upwind rotor, the inflow component is reduced by the superposed effect of the rotation of the rotor, which corresponds to $v_{vortex} < 0$ for a common clockwise rotating rotor. If the upwind rotor rotates counterclockwise, the inflow component is amplified as $v_{vortex} > 0$ increasing $v_{inflow} > 0$ (Fig. 1(a)).

A similar difference can be seen in the averaged w-component (Fig 5 (right column)). In the northern rotor half (Fig. 5(d)) (which is on the left while looking from upstream down on the second rotor), $w_{vortex} < 0$ for a common clockwise rotating rotor, whereas $w_{vortex} > 0$ for a counterclockwise rotating rotor. As $w_{inflow} \approx 0$, the pattern is nearly symmetric at the first rotor position. The same explanation with the opposite sign of w_{vortex} is valid in the southern rotor half (Fig. 5(f)).

This results in rotor averaged differences of v_{wake} (Fig. 5(b)) and w_{wake} (Fig. 5(e)) between clockwise and counterclockwise rotating rotors, which are responsible for the observed difference in streamwise velocity and turbulence kinetic energy and therefore the power output and loading differences at the second turbine.

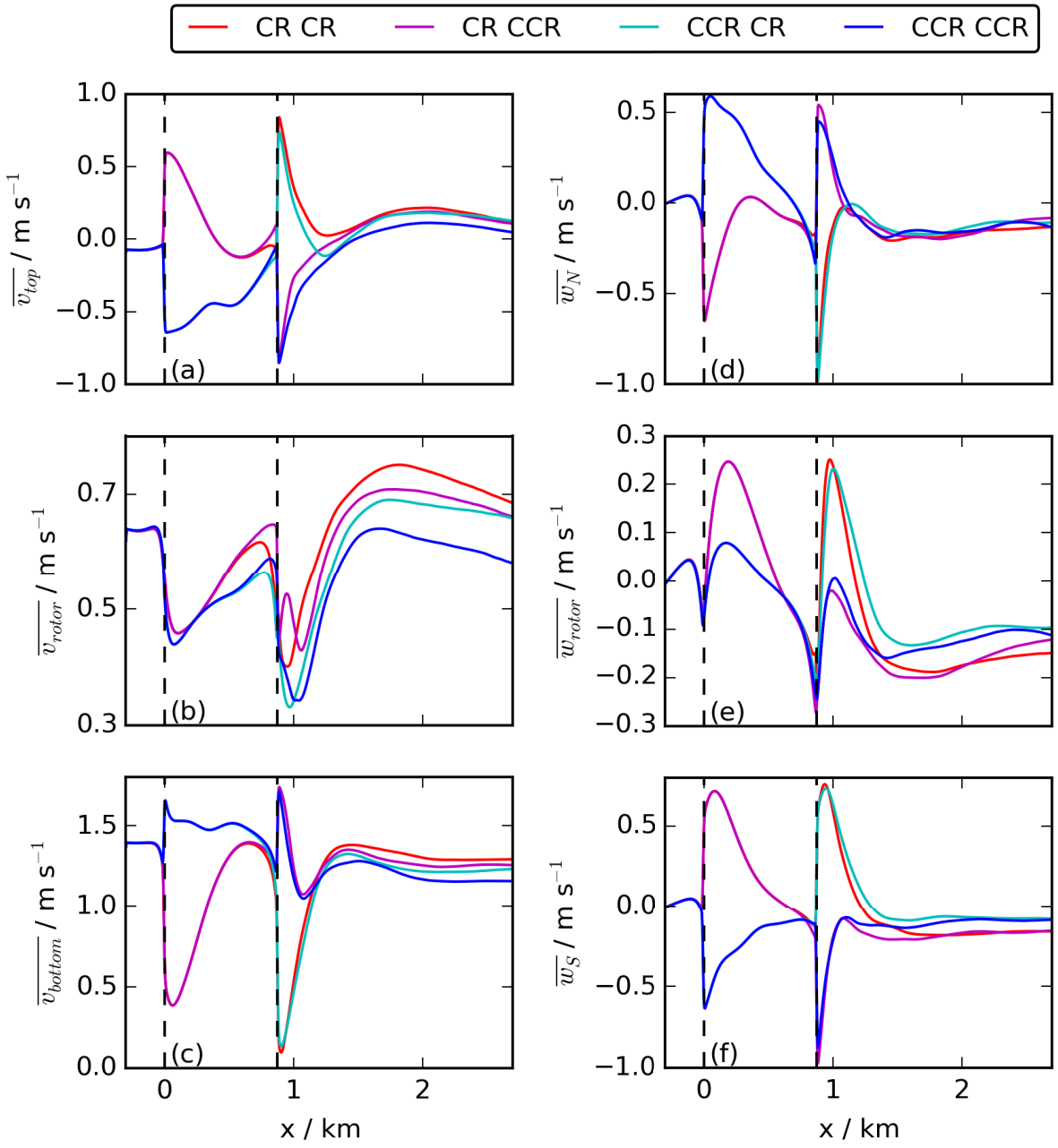

Figure 5: Downstream evolution of the spanwise velocity averaged over the top (a) and bottom (c) rotor half, as well as the average over the whole rotor area (b). The downstream evolution of the vertical velocity averaged over the northern part (d) and the southern part (f), as well as the rotor average (e). The vertical dashed lines are the rotor positions.

3.4 Four wind turbines in a row

The above presented results lead to the reasoning that a counterclockwise rotating upwind turbine would be preferable for the downwind turbines power output (Table 2). Considering a wind farm, many wind turbines are in the wake of an upwind one. A first step towards the investigation of the rotational direction impact on a wind farm under veering inflow is performed with a simulation of

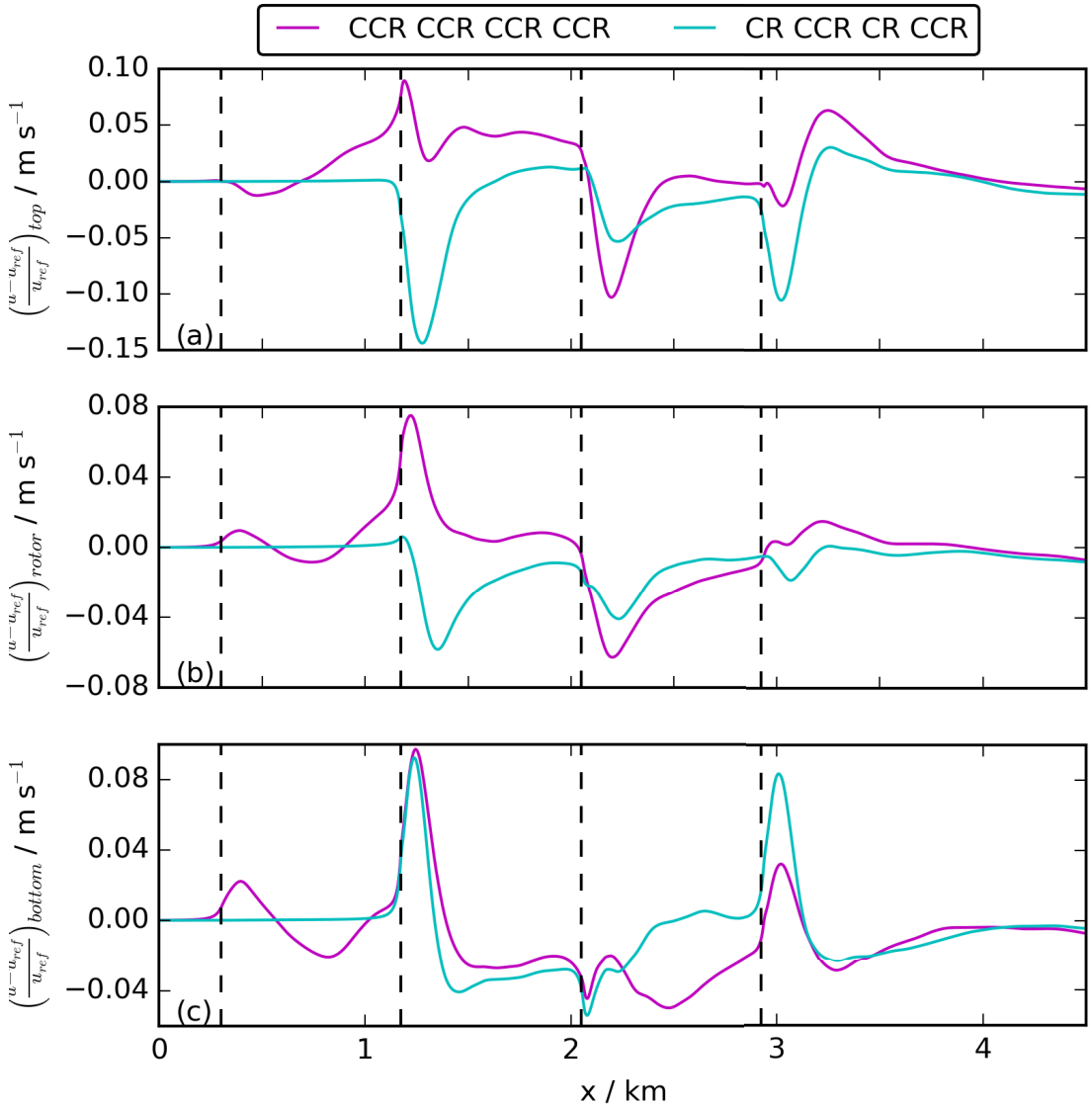

Figure 6: Downstream evolution of the velocity fraction $^{u-u_{ref}}/_{u_{ref}}$. The first row represents the rotor top average, the last row the rotor bottom average, and the centered one the average over the whole rotor. The vertical dashed lines are the rotor positions of the four wind turbines.

four wind turbines in a row. In the reference simulation, all four NREL rotors rotate clockwise. This is compared to four counterclockwise rotating rotors (CCR CCR CCR CCR) and a wind-turbine row with an alternating rotational direction, starting with a common clockwise one (CR CCR CR CCR). The streamwise evolution of the fraction $^{u-u_{ref}}/_{u_{ref}}$ is presented in Figure 6. At the location of the second rotor, the results are identical to Fig. 3(a) - (c), which show an increase of the possible power output in case of a counterclockwise rotating upwind turbine. Considering the performance at the third and fourth wind-turbine positions (dashed vertical lines), the fraction $^{u-u_{ref}}/_{u_{ref}}$ is rather similar for all three arrangements. Transferring this result to the wind farm performance issue, the rotational direction of the upwind turbine has the main impact on the inflow wind speed and

turbulence kinetic energy at the second turbines position. The relative cumulative power production of Table 2 shows therefore a higher value in case of a counterclockwise rotating upwind rotor in comparison to a clockwise rotating one, similar as it is the case with two wind turbines in a row. The percentage difference to the reference case of only clockwise rotating turbines, however, decreases, as the rotational direction impact of the third and fourth wind turbine diminishes.

4 Conclusion

We investigate the impact of the rotational direction of two 5 MW NREL rotors with a turbine spacing of 7 D on the performance of the downwind turbine under veering inflow in an SBL. We carry out LESs for the four possible combinations of rotational direction of two rotors by applying a stably stratified precursor LES as inflow field. The rotational direction impact on the wake of a turbine is consistent with previous investigations [5, 4], resulting in a smaller wake elongation, a larger spanwise wake width, and a larger wake deflection angle for a counterclockwise rotating rotor in comparison to a clockwise rotating one. The performance (rotor averaged streamwise velocity and turbulence kinetic energy) of the downwind turbine is influenced by these rotational direction dependent differences of the upwind rotor on its wake, resulting in a 4.1% increase of the rotor averaged inflow velocity at the downwind rotor, if the upwind rotor rotates counterclockwise in comparison to a common clockwise rotating one. In case of two counterclockwise rotating rotors, the increase is 4.5%. This increase in case of a counterclockwise rotating upwind rotor is accompanied by a 3.7% increase of the rotor averaged turbulence kinetic energy. Therefore, this work suggests to consider the rotational direction as active control mechanism of upwind turbines [11] for the benefit of downwind power output (+4.8% in the considered case), similar as it is done by yawing of upwind turbines.

Transferring these results to a wind farm, we investigate the performance dependence of four wind turbines in a row. The difference in the power output is dominated by the rotational direction impact of the upwind turbine on the second wind turbine. No significant rotational direction impact can be investigated on the third and fourth wind turbine in case of an unstaggered turbine arrangement. The prevailing higher power output in case of a counterclockwise rotating upwind turbine is therefore caused by the interaction of the rotational direction of the upwind turbine with veering inflow.

The atmospheric situation of a wind direction change with height as considered in this study occurs in almost every night both onshore [9, 13] and offshore [10]. The occurrence of a clockwise or a counterclockwise wind rotation with height depends on meteorological conditions and is also location specific. Measurements [9, 13] showed the occurrence of a clockwise wind rotating with height in the Northern Hemisphere, as considered in this study, in three out of four nights, whereas the strength of the directional shear also depends on meteorological conditions and topography. Therefore, our simulations represent a particular situation and real-world conditions certainly modify the strength of the impact on performance. However, as long as the wind direction changes over the height of the rotor, the spanwise flow component behaves differently for both rotational directions, which has an impact on power and loads of the neighbouring turbine.

References

[1] A. Englberger and A. Dörnbrack. Impact of neutral boundary-layer turbulence on wind-turbine wakes: A numerical modelling study. *Boundary-Layer Meteorology*, 2017.

[2] A. Englberger and A. Dörnbrack. Impact of the diurnal cycle of the atmospheric boundary layer on wind-turbine wakes: a numerical modelling study. *Boundary-layer meteorology*, 2018.

[3] A. Englberger and J. K. Lundquist. How does inflow veer affect the veer of a wind-turbine wake? In *North American Wind Energy Academy 2019 Symposium*. Virginia Tech, 2019.

[4] A. Englberger et. al. Changing the rotational direction of a wind turbine under veering inflow: a parameter study. *Wind Energy Science*, 2020.

[5] A. Englberger et. al. Does the rotational direction of a wind turbine impact the wake in a stably stratified atmospheric boundary layer? *Wind Energy Science*, 2020.

[6] F. Mühle et al. The effect of rotational direction on the wake of a wind turbine rotor–a comparison study of aligned co-and counter rotating turbine arrays. *Energy Procedia*, 2017.

[7] J. D. Mirocha et al. Implementation of a generalized actuator disk wind turbine model into the weather research and forecasting model for large-eddy simulation applications. *J Renew Sust Energy*, 2014.

[8] J. M. Prusa et al. EULAG, a computational model for multiscale flows. *Computers & Fluids*, 2008.

[9] K. Walter et al. Speed and direction shear in the stable nocturnal boundary layer. *Journal of Solar Energy Engineering*, 2009.

[10] N. Bodini et al. Offshore wind turbines will encounter very low atmospheric turbulence. In *Journal of Physics. Conference Series*, 2020.

[11] P. Fleming et al. Initial results from a field campaign of wake steering applied at a commercial wind farm–part 1. *Wind Energy Science*, 2019.

[12] P. K. Smolarkiewicz et al. Building resolving large-eddy simulations and comparison with wind tunnel experiments. *J Comput Phys*, 2007.

[13] M. Sanchez Gomez and J. K. Lundquist. The effect of wind direction shear on turbine performance in a wind farm in central iowa. *Wind Energy Science*, 2020.

[14] H. Schmidt and U. Schumann. Coherent structure of the convective boundary layer derived from large-eddy simulations. *J Fluid Mech*, 1989.